Lidar Temperature Measurements During the SOLVE Campaign and the Absence of PSCs from Regions of Very Cold Air

John Burris, Thomas McGee, Walt Hoegy and Paul Newman
Laboratory for Atmospheres, Code 916, Goddard Space Flight Center, Greenbelt, Md. 20771

Leslie Lait, Laurence Twigg and Grant Sumnicht
Science Systems and Applications, Inc., 5900 Princess Garden Parkway, Lanham, Md. 20706

William Heaps
The Instrument Technology Center, Goddard Space Flight Center, Greenbelt, Md. 20771

Chris Hostetler
Radiation and Aerosols Branch, Mail Stop 435, Langley Research Center, Hampton, Va. 23681-2199

Roland Neuber
Alfred Wegner Institute for Polar Research, Telegrafenberg A43, D-14473 Potsdam, Germany

Klaus F. Künzi
Institute for Environmental Physics, University of Bremen, FB1, P. O. Box 330 440, D-28334 Bremen, Germany

Abstract. NASA Goddard Space Flight Center's Airborne Raman Ozone, Temperature and Aerosol Lidar (AROTEL) measured extremely cold temperatures during all three deployments (December 1-16, 1999, January 14-29, 2000 and February 27-March 15, 2000) of the Sage III Ozone Loss and Validation Experiment (SOLVE). Temperatures were significantly below values observed in previous years with large regions regularly below 191 K and frequent temperature retrievals yielding values at or below 187 K. Temperatures well below the saturation point of type I polar stratospheric clouds (PSCs) were regularly encountered but their presence was not well correlated with PSCs observed by the NASA Langley Research Center's Aerosol Lidar co-located with AROTEL. Temperature measurements by meteorological sondes launched within areas traversed by the DC-8 showed minimum temperatures consistent in time and vertical extent with those derived from AROTEL data. Calculations to establish whether PSCs could exist at measured AROTEL temperatures and observed mixing ratios of nitric acid and water vapor showed large regions favorable to PSC formation. On several occasions measured AROTEL temperatures up to 10 K below the NAT saturation temperature were insufficient to produce PSCs even though measured values of nitric acid and water were sufficient for their formation.

Introduction

During the winter of 1999/2000 the Sage III Ozone Loss and Validation Experiment (SOLVE) campaign was carried out concurrently with the Third European Stratospheric Experiment on Ozone (THESEO) to study the processes controlling ozone levels from the polar to mid-latitude stratosphere. A second objective for SOLVE was to provide the correlative measurements necessary to validate the Stratospheric Aerosol and Gas Experiment (SAGE III) satellite instrument. Temperature was a key measurement for both the expected satellite validation and its impact upon Polar

Stratospheric Clouds (PSCs). PSCs play a central role in the loss of Arctic ozone by providing surfaces on which inactive reservoir species are converted to active species capable of destroying ozone. Their formation depends critically upon an air parcel's temperature and time history, its altitude and the mixing ratio profiles of nitric acid and water vapor. Because of temperature's pivotal role in the formation and duration of PSCs, NASA Goddard Space Flight Center flew a new lidar on the DC-8 to provide temperature profiles at high vertical resolution. Lidar retrievals from an aircraft platform offer distinct advantages over a satellite by providing high precision temperature profiles coincident with measurements of ozone, aerosols, clouds and water vapor throughout the region of interest. These measurements were designed to help understand under what conditions PSCs form and persist by identifying regions in the lower Arctic stratosphere where temperatures dropped below the local saturation point. In this paper we present profiles of extremely cold temperatures made by the Airborne Raman Ozone, Temperature and Aerosol Lidar (AROTEL) from the DC-8. Comparisons are made between these cold temperature measurements and those retrieved by balloon sondes. Resulting comparing PSC observations by the Langley Research Center's (LaRC) Aerosol Lidar with calculations showing locations favorable to the existence of PSCs as a function of $T_{nat} - T_{arotel}$ and measured values of nitric acid and water vapor are presented.

Instrument

AROTEL is a combined aerosol, ozone and temperature lidar designed for operation on an aircraft platform such as the DC-8. AROTEL's design utilized a proven hardware configuration that has been successfully implemented on other Goddard ground based and airborne lidars. AROTEL employed two lasers, a xenon chloride excimer operating at 308 nm and a Nd:YAG with outputs at 1064, 532 and 355 nm. A differential absorption measurement of stratospheric ozone was made using the 308 and 355 nm wavelengths and is the subject of a companion paper is this issue of JGR. Temperatures were retrieved using elastic (Rayleigh) molecular scattering at 355 nm and inelastic (Raman) scattering at 387 nm (from 355 nm). The Raman channel originates with inelastic scattering off of molecular nitrogen having an energy shift of ~2331 cm^{-1}. Signals were captured using a telescope with a 40 cm diameter primary mirror. They were then separated into their constituent wavelengths using beam splitters and bandpass filters with high out of band blocking. Gated photomultipliers (PMTs) were used for signal detection on all UV channels because of their sensitivity, linearity and low noise. Non-linear behavior in the PMT's gain and signal induced noise were minimized by limiting the detected signal's dynamic range associated with any one PMT to less than five orders of magnitude. Analog signal detection was implemented for returns originating within 1 km of the aircraft while photon counting was employed to beyond 60 km. This configuration permitted both a compact design and high detector throughput but, because of the relatively large filter bandpass, limited temperature retrievals to solar zenith angles (SZAs) $\geq$85 degrees. Temperature retrievals to 60 km were made for SZA's $\geq$95 degrees, for SZA's less than 95 degrees the maximum reportable altitude was progressively reduced as the SZA decreased due to interference from the sun. A more detailed description of the AROTEL instrument can be found in *McGee et al* [this issue].

Measurement Technique

Temperature profiling via lidar is a well established technique that has been successfully employed for many years [*Gross et al.*, 1997; *Hauchecorne and* Chanin, 1980; *Leblanc et al.*, 1998]. For the temperature measurement, AROTEL used a Nd:YAG laser that produced between 200-300 millijoules at 355 nm at a pulse repetition rate of 50 Hz. The large UV backscattering cross sections maximized signal returns without interference from ozone absorption. Data was acquired using both elastic and inelastic scattering. Inelastic scattering enhanced AROTEL's retrieval capabilities in the presences of clouds and aerosols because of the negligible impact Mie scattering had on this channel; the 387 nm channel was also insensitive to the strong fundamental returns at 308 nm. Temperatures both within and below clouds, PSCs, and aerosol layers have been successfully derived from the inelastic data provided the optical depth is not high (a paper discussing temperature retrievals in the presences of clouds is in preparation). When compared to ground based lidar systems an aircraft platform at flight altitude experiences less signal attenuation by operating above the troposphere and a major enhancement in return signals through minimizing the $range^{-2}$ loses. Temperature

retrievals were made within a much shorter time period than is possible from a much larger, ground-based, lidar system.

Both elastic and inelastic returns were directly proportional to atmospheric number density. Removal of the signal's range^{-2} dependence provided a relative measurement of atmospheric density when tied to a model; absolute densities could be recovered by normalizing the measured profile against a balloon sonde measurement of density at a reference altitude. Because Rayleigh scattering introduces significant signal attenuation in the UV, a correction for it was made for all altitudes using the calculated density profile. Elastic returns require a correction for Mie scattering below altitudes of ~22-25 km, otherwise inelastic data must be employed for a temperature retrieval. In recent years stratospheric lidar retrievals have benefitted from the natural removal of volcanic aerosols injected by the eruption of Mt. Penatubo in 1991; the presence of these volcanic aerosols had made retrievals difficult below ~30 km. Temperature profiles are derived from the measured atmospheric densities utilizing the ideal gas law [PV = nkT] and the assumption that local hydrostatic equilibrium ($dP/dz = \rho g$) prevails. It is important to note that temperature profiles are retrieved using changes in relative, not absolute, number density. The resulting temperature derivation is thus insensitive to the absolute values for a number of instrumental parameters including detector transmission efficiency, photocathode quantum efficiency, laser output power and size of the telescope's primary mirror. These parameters, however, do affect count rates and hence measurement uncertainties. The derived temperature at a geometric altitude z_i is given

$$T(z_i) = T(z_0) * \frac{n_0}{n_i} + \frac{M}{R} \sum_{j}^{i} \frac{g_j n_j \Delta z_j}{n_0} \quad (1)$$

where z_0 is the tie-on altitude, n_j the measured atmospheric number density, M the average molecular mass, R the gas constant, g the gravitational constant and Δz the measurement interval. The temperature algorithm must be initialized at the highest measurement point (typically between 50-60 km for AROTEL) employing either a pressure or temperature tie-on; temperature was employed by AROTEL.

Errors

Errors in retrieved temperature arise from a number of sources. For reported temperatures above ~40 km, uncertainties associated with the tie-on temperature exert a major impact. The retrieval algorithm is initialized using either the CIRA86 model (at 60 km geometric altitude) or the Goddard Data Assimilation Office temperature product (at the 0.5 mbar pressure level). DAO temperatures could be obtained in advance of a flight for use in real time retrievals once the flight track had been determined. The errors for this data set using a tie-on at the 0.5 mbar pressure level (~55 km) are reported to be ≤5K [*Steve Pawson, private communication*]. The CIRA86 model is based on climatology with both monthly and zonal average temperatures, pressures and densities from 0 to 120 km in 5 km intervals. Observed differences between DAO and CIRA86 were generally less than 10 K at the tie-on altitude. This error is negligible three scales heights (~20 km) below the tie-on point. A tie-on at 60 km with an uncertainty of ΔT generated a residual error of $\sim\Delta T^*\exp(-3)$ at 40 km. Since the DAO tie-on at 0.5 mbar was generally better than 5 K, residual tie-on errors at 40 km were typically ≤0.3 K. For the CIRA86 model an uncertainty of 15 K at 60 km introduces a tie-on error of ~0.7 K at 40 km. Counts derived from other than molecular backscattering are another error source. These include dark counts from the PMTs and those generated by light sources whose output was within the bandpass of AROTEL's detectors. Background counts were subtracted from the acquired data before deriving temperatures. Under normal conditions the background count rate is linear with time and can be calculated by averaging counts in channels sufficiently distant in time such that no backscattering is observed. However for certain conditions intense signal returns can drive the background rate non-linear and require the use of a fitting function to characterize its behavior as a function of time. Although not important at high data rates this significantly increases measurement uncertainties at low signal levels. Statistical uncertainties associated with photon counting can exert a major impact for the low signal levels typically seen at the maximum altitude range of each data channel. These errors are reduced by integrating returns over a longer time period, decreasing the vertical resolution and smoothing the

resulting data. Smoothing removes high frequency noise associated with the data but increases the vertical scale of the measurement. Photon counting at high data rates can saturate both discriminators and counting electronics. A correction for these induced non-linearities was employed in the retrieval algorithm. Additional error sources include uncorrected extinction due to aerosols and clouds [to be discussed in greater detail in an upcoming paper]. Reported errors in AROTEL temperature as a function of altitude for the SOLVE mission are given in Figure 1. A comprehensive treatment of both the temperature retrieval technique and associated errors is given in *Gross et al.*[1997].

Intercomparison

AROTEL temperatures were compared to those retrieved by both balloon sondes and the Meteorological Measurement System (MMS) during SOLVE [*Burris et al.*, this issue]. For the sonde comparisons a coincidence was defined as occurring when the DC-8 flew no farther than 100 km from the launch site within 12 hour of the retrieval. There were 28 separate profiles of elastic temperatures that meet this criterion, 23 were used for the inelastically derived temperature comparison. Elastically derived temperatures were ~1.1±0.6 K colder than sonde values while inelastic retrievals averaged ~1.2±1.1 K colder than sonde values. MMS made continuous in-situ temperature measurements at the ER-2's flight altitude. Coincidence between AROTEL and MMS existed for measurements acquired within 30 km of each another on the same flight date. Analysis of data from three separate flights showed AROTEL was from 2 to 3 degrees colder than reported MMS values for both elastic and inelastically derived temperatures.

AROTEL Temperature Measurements During SOLVE

AROTEL temperature profiles are calculated from the aircraft to ~60 km in 150 meters intervals with 0.5-1.5 km vertical resolution. The horizontal footprint ranged from 4 to 70 km depending on the integration time and signal to noise ratio. Temperatures are reported in geometric altitude and are available at URL: http://hyperion.gsfc.nasa.gov/Public/Ground_based/arotel/solve1. During the first deployment, the DC-8's geometric altitude was provided by the DADS (Data Acquisition and Distribution System) GPS system with a stated precision of ±50 meters. During the second and third deployments a differential GPS altitude was available via post processing of the flight data with a reported accuracy of ±1 meter over most of the DC-8's flight track [*Carl Sorenson, private communication*]. Temperatures derived from elastic backscatter data are reported for altitudes from the aircraft to approximately 45 km, inelastic scattering data was employed for retrievals from the aircraft to between 20 - 25 km depending on local conditions. During the winter of 1999-2000 low temperatures were observed throughout the Arctic polar region (Figure 2). Regions of very cold air were repeatedly observed by AROTEL during all three SOLVE deployments. Temperatures at or below 192 K were retrieved on many dates with extensive regions being observed during flights on December 7, 1999, December 10, 1999, December 12, 1999, January 14, 2000, January 16, 2000, January 20, 2000, January 23, 2000, January 25, 2000, January 27, 2000 and March 5, 2000. Localized temperatures at or below 188K were also frequently observed with particularly widespread regions occurring during flights on December 12, January 20, January 23 and January 25. In regions having only background stratospheric aerosols, as determined by AROTEL and LaRC data, low temperatures were derived utilizing both elastic and inelastic backscatter signals (Figures 3 and 4 display both elastic and inelastically derived temperatures for December 12 when minimal PSC activity was observed by the LaRC Aerosol Lidar). Temperatures below 191 K existed over a large area for altitudes ranging from ~18 km to almost 30 km on flight date December 12. The DC-8's flight track on December 12th (Figure 5) show the large area over which the temperature soundings were made on this date. Figures 6 and 7 display both elastic and inelastically derived temperatures between 185 and 195 K, at 2 K resolution, with significant structure in the temperature fields evident in both retrievals. Broad areas between 187 and 189 K are seen from 20-26 km altitude and, in some cases, extending over 800 km (~1 hour flight time) horizontally. Differences between

temperatures retrieved employing elastic and inelastic returns as a function of altitude were calculated for December 12 and are displayed in Figure 8; the mean differences between 20 and 25 km was ~0.3% which is ~0.6 K at 200 K. These small differences were due to the absence of PSCs and the resulting Mie interference on the elastic channel.

The strong influence exerted by PSCs on retrieved temperature is displayed in Figure 9 for the flight on December 7. Between 1230 and 1430 GMT the DC-8 flew beneath a cloud observed by the LaRC Aerosol Lidar (Figure 10). Both inelastic and elastically retrieved temperatures within the PSC are shown. 1-sigma uncertainties are presented for both retrieved temperatures. The vertical extent of the cloud, as determined from its impact on the temperature retrieval, ranged from ~21 to 23 km and is consistent with the data provided by LaRC. Figure 11 provides a difference plot of temperatures derived by elastic and inelastic scattering as a function of altitude. The maximum temperature difference within the cloud between elastic and inelastic scattering was -12 K Figure 12 displays the backscattering ratio (BSR - defined as $(\beta_{rayleigh} + \beta_{aerosol})/\beta_{rayleigh}$) at 355 nm as a function of altitude. Within the cloud it attained a peak value of ~1.07 which corresponds to an optically thin PSC. The cloud's optical properties as measured by the LaRC Aerosol Lidar are consistent with its identification as a type Ia PSC. Plots of both elastic and inelastically determined temperature for the same date but just outside the cloud are given in Figure 13. Differences were generally less than ~2 K for altitudes ranging between 18 and 28 km. The mean temperature difference between inelastic and elastically determined temperatures was -0.2 ± 1.5 K. Figure 14 displays a high resolution temperature plot of elastically derived temperatures for the December 7 flight date. Slightly warmer temperatures were observed on this flight and they lacked the extensive vertical and horizontal structure seen on December 12 (Figures 6 and 7).

Temperature retrievals are currently possible for backscattering ratios (at 355 nm) that are less than approximately 1.5. Within clouds and aerosol layers having larger BSR values retrievals are not feasible with this technique unless a correction for extinction is included. The issue of using inelastically scattered returns to derive temperatures within optically thin clouds and aerosols is addressed in a companion paper in this issue [*Twigg et al.*].

Balloon Sonde Temperature Measurements

AROTEL repeatedly encountered temperatures at or below 187 K during SOLVE. Temperatures this cold are infrequently observed in the Arctic because the polar vortex is neither as stable nor long lived as in the Antarctic. Although few satellite measurements were available, numerous balloon sondes were launched during SOLVE that provided a detailed, continuous, record of temperatures to beyond ~25 km altitude. The cold temperatures encountered in the Arctic winter caused the balloons to burst before reaching their maximum altitude and permitted only sporadic sampling above ~25 km even when special techniques were employed to protect the balloons. These measurements occurred both within and without the polar vortex and generally covered the critical band between 18 and 25 km where PSCs were most frequently observed by the LaRC Aerosol Lidar. This study encompassed a region regularly traversed by the DC-8 during SOLVE although these sonde measurements were not generally coincident with those of AROTEL. Nonetheless, these sonde temperature records permit an independent assessment of the frequency and extent of the very cold temperatures observed by AROTEL throughout the SOLVE deployment. These meteorological sondes were launched from Ny Ålesund (78.9N, 11.9E), Danmarkshaven, Greenland (76.8N, 18.8W), Scoresbysund, Greenland (70.5N, 22.0W), Jan Mayen, Norway (70.9N, 8.7W) , Bjornoya Island, Norway (74.5N, 19.0E) and Keflavik, Iceland (64.0N, 22.6W). All six sites recorded low temperatures throughout the period. Figure 15 presents temperature retrievals by a sonde and AROTEL for inelastically derived temperatures during a coincident measurement; the sonde recorded a minimum temperature of ~189 K at 23 km, AROTEL measured ~188 K at the same altitude approximately 1.5 hours after the sonde's launch. Figure 16 plots the minimum temperature reported by these six sites as a function of date and altitude between November 30th and March 15th. Temperatures below 190 K were regularly seen from about December 15 through early February, 2000. The minimum temperature, 183 K, was observed on January 18 at Danmarkshaven, Greenland. As shown in Figure 16 there was the expected steady downward progression in minimum temperature as the winter progressed. The coldest temperatures were noted for the sites located at Danmarkshave and Scoresbysond, Greenland and Ny Ålesund. The temperatures from mid-December into late January at Danmarkshave, Scoresbysond and Ny Ålesund show very cold temperatures existing from ~20 to 25 km altitude

for a considerable period of time. The picture provided by the sonde data is thus broadly consistent with the AROTEL retrievals in vertical extent, duration and lowest minimum value.

Correlations between observed PSCs to measured low temperatures.

Although temperatures significantly below T_{nat} (Figure 17) were repeatedly encountered, these cold regions did not correlate well with PSC observations made by the LaRC Aerosol Lidar. Localized PSCs were observed on both December 7, December 10, January 16 and January 29; the flight on December 12 showed minimal activity while data from January 20, 23 and 25th showed extensive PSC development. During the December 7 flight, regions with temperatures below 192 K were observed at altitudes ranging from 20 to 30 km for most of the 9 hour flight with PSCs being seen only sporadically. On the December 12 flight, the LaRC Aerosol Lidar reported no activity during five hours of observations while AROTEL observed large regions below 191 K between 20 and 30 km altitude. Temperatures derived using both elastic and inelastic returns frequently showed areas at or below 187 K but again there was no evidence for type I or type II PSCs in either the temperature or PSC record. These observations led to a study to determine where PSCs could exist as a function of temperature below T_{nat} and the local mixing ratios of nitric acid and water.

The scattering ratio ((aerosol + molecular)/molecular) data from the 1064 nm channel of the Hostetler instrument were selected which were co-located with DAO temperatures greater than 200 K. The mean of these warm-air scattering ratios plus four times their standard deviation is calculated as the threshold value below which the ratios are considered to be part of the background noise. In the plots of scattering ratios versus temperature, each measurement is color-coded by whether it is expected to be associated with a PSC. The NAT condensation temperature and the frost point are computed from the Hanson and Mauersberger [1988] criteria using (a) the pressures obtained by converting the analyzed geopotential heights (on pressure surfaces) to geometric heights and interpolating to the lidar profiles, (b) a quadratic best fit to the HNO3 profile data from the ASUR instrument [Mees et al.] for the flight, and (b) a constant H2O value of 5 ppmv (consistent with in situ measurements of stratospheric water vapor made by the Harvard H2O instrument on board the ER-2). If a temperature (AROTEL or DAO) is less than the NAT condensation temperature, the measurement is colored red. If the temperature is less than the frost point, it is colored yellow. Other points are left as gray. Thus, gray points are those for which one would not expect to see PSCs, and red and yellow points are points for which Type I and II PSCs are expected, respectively. Points above the dotted line are those for which scattering ratios were enhanced (i.e., PSCs), and points below the line are part of the background.

The results for December 12, January 16 and January 29 are presented in Figures 18-20 and show regions that are up to 10 K colder than T_{nat} and display no evidence of PSCs. December 12 had areas that are cold enough for type 2 PSCs but no PSCs were observed by the LaRC lidar. The temperature uncertainties for these data sets is typically less than 1 K and for December 12 usually much less. For comparison, DAO temperatures were used to generate plots identical to those using AROTEL temperatures and the regions where PSCs could exist are broadly similar with those of AROTEL.

Discussion:

AROTEL temperature retrievals showed widespread areas of very cold air during all three deployments of the SOLVE campaign. Temperatures below 191 K were regularly encountered over large areas and localized regions at or below 189 K were frequently observed. Minimum temperatures retrieved by meteorological sondes launched during the mission are consistent with those derived from AROTEL data within the Arctic both in time and vertical extent. Comparisons between PSC observations by the LaRC Aerosol Lidar and calculations designed to show whether PSCs could exist based on measured AROTEL temperatures showed large areas where the AROTEL temperature was 4 or more degrees below T_{nat} and yet no PSCs were observed although sufficient water and nitric acid was present.

Acknowledgments. The authors would like to acknowledge the support provided by NASA's Upper Atmosphere Research Program for the Airborne Raman Ozone and Temperature Lidar (AROTEL). We would like to thank the many members of the DC-8 support team at Dryden Flight Research Center for their support in all facets of the instrument's installation and operation. Don Silbert did a superlative job of keeping both lasers and computers operational during the many critical hours of airborne operation.

References:

Burris, J. T.J. McGee, W. Hoegy, L. Lait, L. Twigg, G. Sumnicht, W. Heaps, T.P.Bui, R. Neuber, Validation of Temperature Measurements from the Airborne Raman Ozone Temperature and Aerosol Lidar During SOLVE, *this issue of JGR.*

Gross, M., T.J. McGee, R.A. Ferrare, U.N. Singh and P. Kimvilakani , Temperature measurements made with a combined Rayleigh-Mie and Raman lidar, *Appl. Opt.* 36, 5987-5994, 1997.

Hanson, D., and K. Mauersberger, Laboratory studies of the nitric acid trihydrate: Implications for the south polar stratosphere, *Geophys. Res. Lett.*, 15, 855-858, 1988.

Hauchecorne, A., and M.L. Chanin, Density and temperature profiles obtained by lidar between 35 and 70 km, *Geophys. Res. Lett.*, 8, 565-568, 1980.

Kawa, S. R., D. W. Fahey, K. K. Kelly, J. E. Dye, D. Baumgardner, B. W. Gandrud, M. Loewenstein, G. V. Ferry and K. R. Chan, The arctic polar stratospheric cloud aerosol: aircraft measurements of reactive nitrogen, total water and particles, *J. Geophys. Res.*, 97, 7925-7938, 1992.

Leblanc, T., I. S. McDermid, A. Hauchecorne and P. Keckhut, Evaluation of optimization of lidar temperature algorithms using simulated data, *J. Geophys. Res.*, 103, 6177-6187, 1998.

McGee, T. J., J. Burris, L. Twigg, Wm. Heaps, G. Sumnicht, W. Hoegy and C. Hostetler, AROTEL: An Airborne Ozone, Aerosol and Temperature Lidar, this issue.

Mees, J., S. Crewell, H. Nett, G. Gelange, H. Vandestadt, J. J. Kuipers and R.A.Panhuyzen, ASUR - An Airborne SIS Receiver for Atmospheric Measurements of Trace Gases at 625 TO 760 Ghz, IEEE Trans. Microwave Theory and Tech. 43: (11) 2543-2548, 1995.

Figure Captions

Figure 1. Calculated temperature uncertainties for both Rayleigh (elastic) and Raman (inelastic) temperatures derived on flight date 991207 as a function of altitude. The large change observed in elastically derived temperature uncertainties at 26 and 39 km is due to changing from a mid-altitude to high altitude channel. Significantly more signal is directed towards the high altitude channel to extend its vertical range - at lower altitudes this translates into higher count rates (and lower measurement uncertainties).

Figure 2. Minimum reported temperatures within the Arctic for the 1999-2000 winter at 30 hPa (~23 km). The minimum temperature observed was 183 K in mid-January.

Figure 3. Elastic temperatures retrieved for flight date 991212. Temperatures were calculated from data acquired with five minutes of integration . After smoothing the vertical resolution varied from 0.5 to 1.5 km.

Figure 4. Inelastic temperatures for flight date 991212. Temperatures cover the same flight track as in figure 3 but are limited to altitudes below ~25 km.

Figure 5. DC-8's flight track for 991212. This flight provided data over a large area with minimal overlap.

Figure 6. High resolution elastic temperatures between 185 K and 195 K for 991212. Large regions below 191 K are visible for most of the flight.

Figure 7. High resolution inelastic temperature retrievals between 185K and 195 K for 991212. Extensive areas below 189 K are seen throughout the flight.

Figure 8. Differences between elastic and inelastically derived temperatures for 991212 calculated between 13 and 25 km altitude and averaged over the entire flight. From 20 through 25 km the differences averaged <0.3%.

Figure 9. Elastic (solid squares) and inelastically (open squares) derived temperatures acquired within an optically thin PSC on 991207. 1-sigma uncertainties are shown.

Figure 10. PSC profiles as a function of time (GMT) and altitude for flight date 991207.

Figure 11. Differences between elastic and inelastically derived temperatures acquired simultaneously within an optically thin PSC on 991207.

Figure 12. Backscatter ratio at 355 nm within an optically thin PSC on 991207. The peak value of ~1.07 identifies this as an optically thin cloud.

Figure 13. Elastic (open squares) and inelastically (solid squares) derived temperatures just outside the PSC detected on 991207.

Figure 14. High resolution elastic temperatures between 185 K and 195 K for flight date 991207. Although PSCs were observed temperatures were not as cold on this date as on 991212.

Figure 15. Balloon sonde and AROTEL temperatures (inelastically derived data) for 991212. The AROTEL

profile was acquired at 17.36 GMT, the sonde was launched from Ny Ålesund at 16.03 GMT. The minimum sonde temperature was ~189 K at 23 km, AROTEL measured ~188 K for this altitude.

Figure 16. Plot of minimum temperatures versus date and altitude for sondes launched from Ny Ålesund (78.9N, 11.9E), Danmarkshaven, Greenland (76.8N, 18.8W), Scoresbysund, Greenland (70.5N, 22.0W), Jan Mayen, Norway (70.9N, 8.7W), Bjornoya Island, Norway (74.5N, 19.0E) and Keflavik, Iceland (64.0N, 22.6W) from November 30, 1999 through March 15, 2000.

Figure 17. Plots of T_{nat} (dashed line) and T_{sat} (dot-dash line) as a function of altitude for representative mixing ratios of water and nitric acid. The solid line was a representative temperature retrieved by AROTEL, the dotted line is the US Standard Atmosphere's temperature.

Figure 18. The upper left plot is of LaRC backscatter data at 1064 nm used to identify PSCs. None were visible during the operation of the LaRC lidar on 991212. The upper right plot is of AROTEL temperatures for the same altitude range as the LaRC data. The lower left plot displays the backscatter ratio data measured by LaRC as a function of $T_{AROTEL} - T_{NAT}$. The red area highlights conditions where type 1 PSCs could exist for AROTEL temperatures and measured values of nitric acid and water. The yellow region highlights where type 2 PSCs could exist. The dotted line delineates the regions where PSCs were observed from where they were not. The lower right plot is identical to that on the left except for the use of DAO, rather than AROTEL, temperatures for the PSC existence calculation.

Figure 19. The upper left plot is of LaRC backscatter data at 1064 nm used to identify PSCs. The upper right plot is of AROTEL temperatures for the same altitude range as the LaRC data. The lower left plot displays the backscatter ratio data measured by LaRC as a function of $T_{AROTEL} - T_{NAT}$. The red area highlights conditions where type 1 PSCs could exist for AROTEL temperatures and measured values of nitric acid and water. The yellow region highlights where type 2 PSCs could exist. The dotted line delineates the regions where PSCs were observed from where they were not. The lower right plot is identical to that on the left except for the use of DAO, rather than AROTEL, temperatures for the PSC existence calculation.

Figure 20. The upper left plot is of LaRC backscatter data at 1064 nm used to identify PSCs. The upper right plot is of AROTEL temperatures for the same altitude range as the LaRC data. The lower left plot displays the backscatter ratio data measured by LaRC as a function of $T_{AROTEL} - T_{NAT}$. The red area highlights conditions where type 1 PSCs could exist for AROTEL temperatures and measured values of nitric acid and water. The yellow region highlights where type 2 PSCs could exist. The dotted line delineates the regions where PSCs were observed from where they were not. The lower right plot is identical to that on the left except for the use of DAO, rather than AROTEL, temperatures for the PSC existence calculation.

Summary of paper designed for the general public.

Lidar Temperature Measurements During the SOLVE Campaign and the Absence of PSCs from Regions of Very Cold Air

During the winter of 1999/2000 a scientific expedition, the SAGE III Ozone Loss and Validation Experiment (SOLVE) campaign, was mounted to study ozone loss in the upper Arctic atmosphere. Goddard Space Flight Center flew an instrument on NASA's DC-8, the Airborne Raman Ozone, Temperature and Aerosol Lidar (AROTEL), consisting of two lasers, a telescope and electronics designed to measure ozone, temperatures and aerosols at distances up to ten miles above the aircraft. AROTEL repeatedly measured very cold temperatures, many were below -117 °F, at altitudes of from 45,000' to 75,000' . Temperatures this cold can, if sufficient water and nitric acid are present, cause high altitude clouds to form which can play a key role in destroying Arctic ozone. Large regions with temperatures below -117 °F were observed with no clouds but sufficient water and nitric acid to allow the formation of these polar stratospheric clouds. These observations suggest that the current understanding of how these clouds form is not complete.

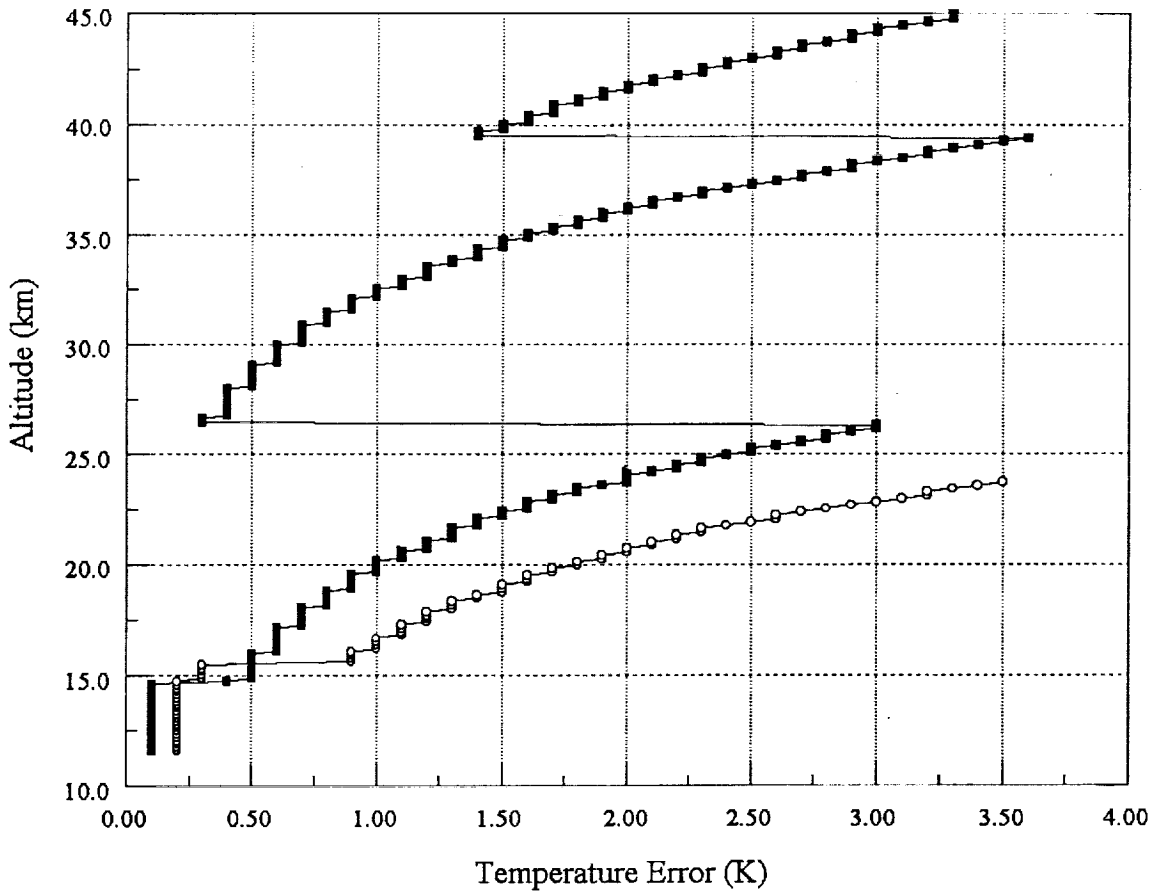

Figure 1 Calculated uncertainties for temperatures derived from both Rayleigh (elastic / solid squares) and Raman (inelastic / open squares) data on flight date 991207 as a function of altitude. The large change observed in elastically derived temperature uncertainties at 26 and 39 km is due to changing between mid-altitude to high altitude channels. Significantly more signal is directed towards the high altitude channel to extend its vertical range - at lower altitudes this translates into higher count rates and (and lower measurement uncertainties).

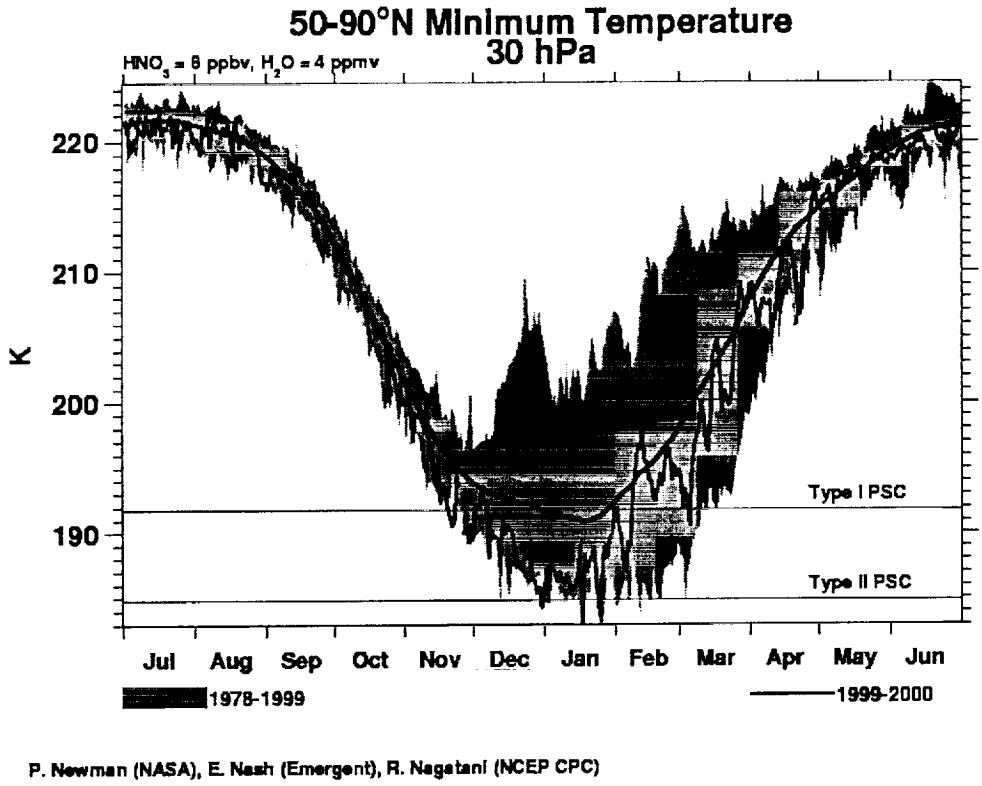

Figure 2 Minimum reported temperatures within the Arctic for the 1999-2000 winter at 30 hPa (~23 km). The minimum temperature observed was 183 K in mid-January.

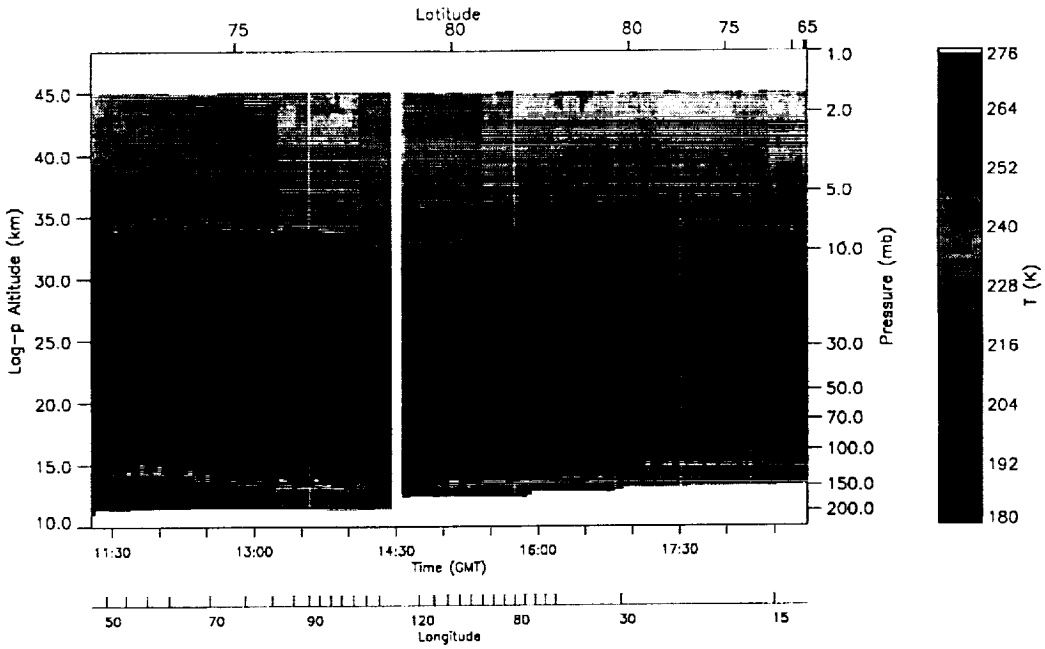

Figure 3 Elastic temperatures retrieved for flight date 991212. Temperatures were calculated from data acquired with five minutes of integration. After smoothing the vertical resolution varied from 0.5 to 1.5 km.

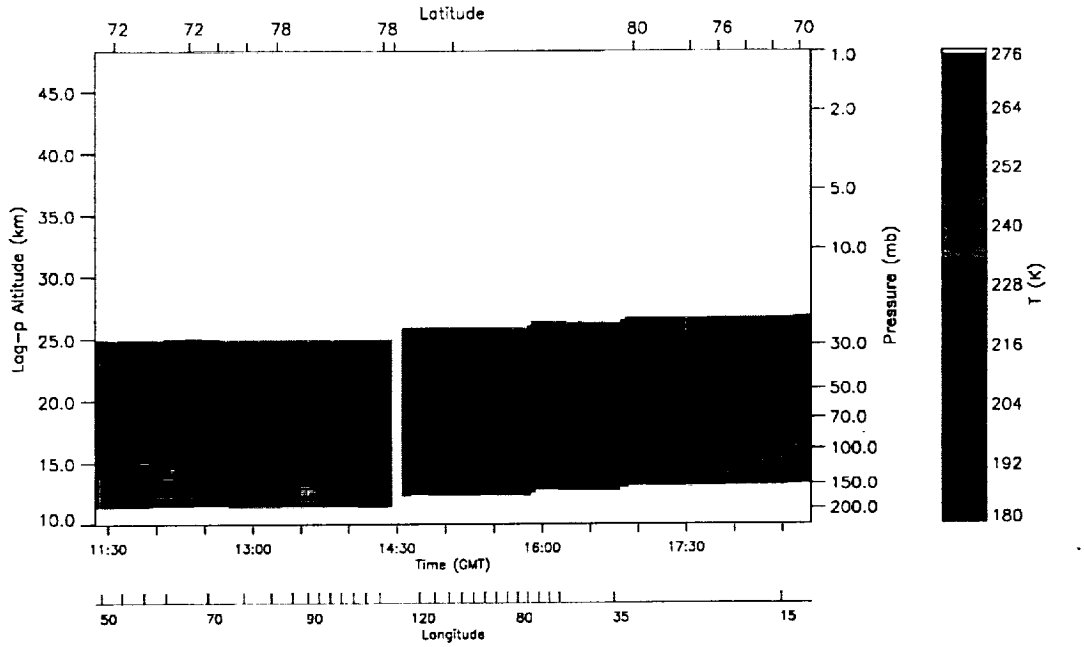

Figure 4 Inelastic temperatures for flight date 991212. Temperatures cover the same flight track as in figure 3 but are limited to altitudes below ~25 km.

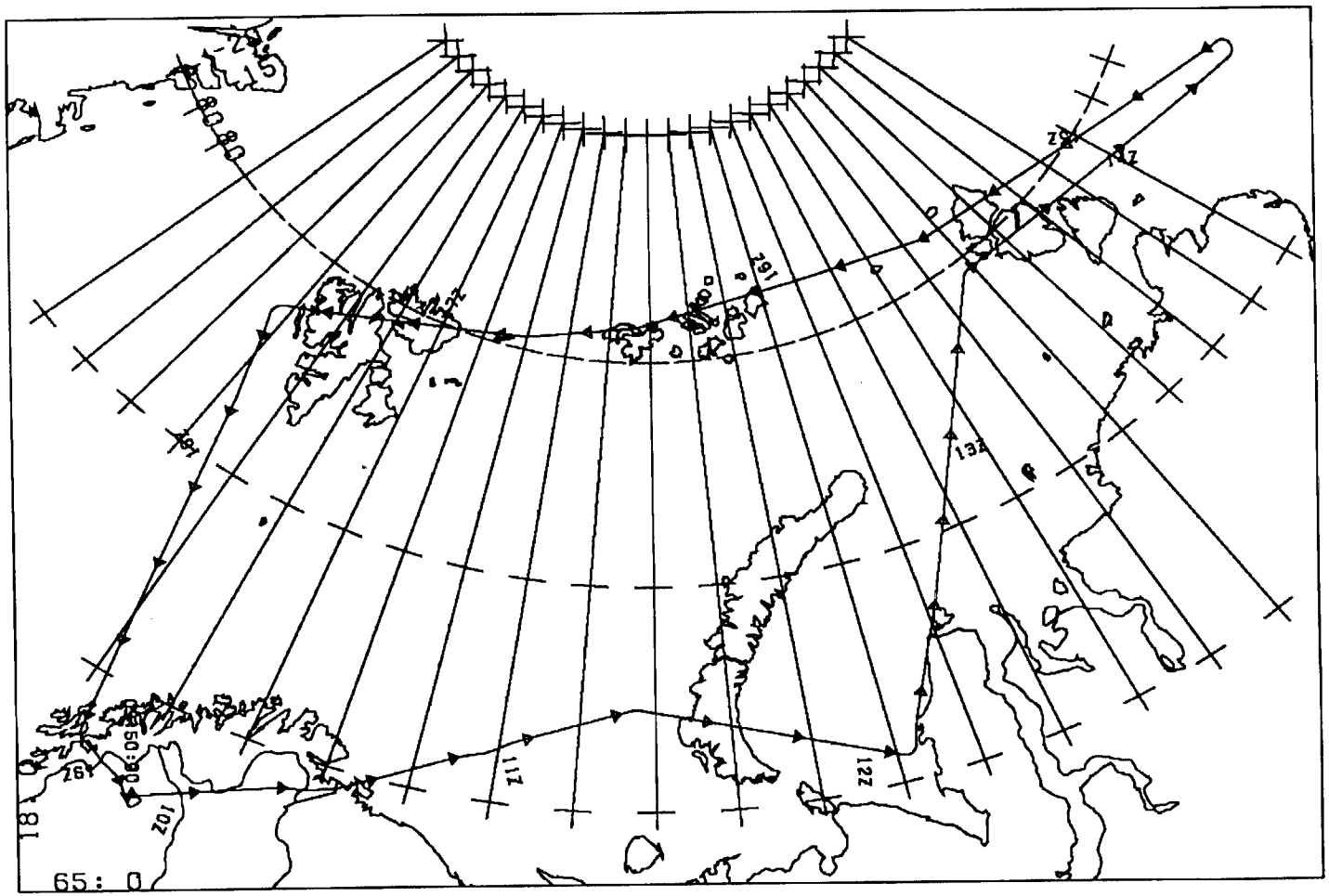

Figure 5 DC-8 flight track for 991212. This flight provided data over a wide area with minimal overlap.

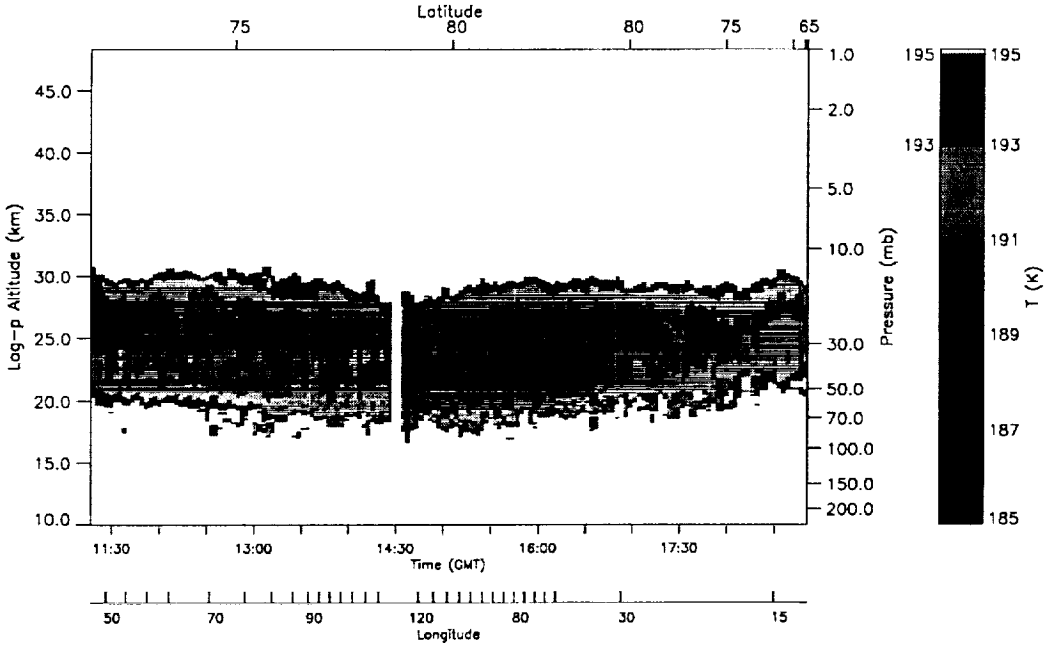

Figure 6 High resolution elastic temperatures between 185 K and 195 K for 991212. Large regions below 191 K are visible for most of the flight.

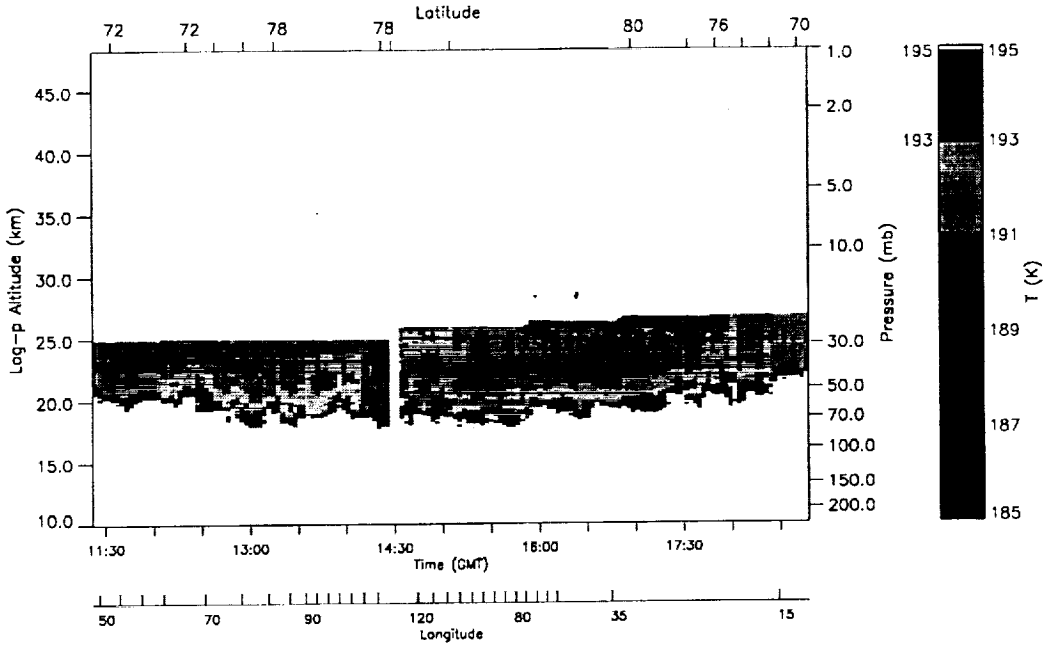

Figure 7 High resolution inelastic temperature retrievals between 185 K and 195 K for 991212. Extensive areas below 189 K are seen throughout the fight.

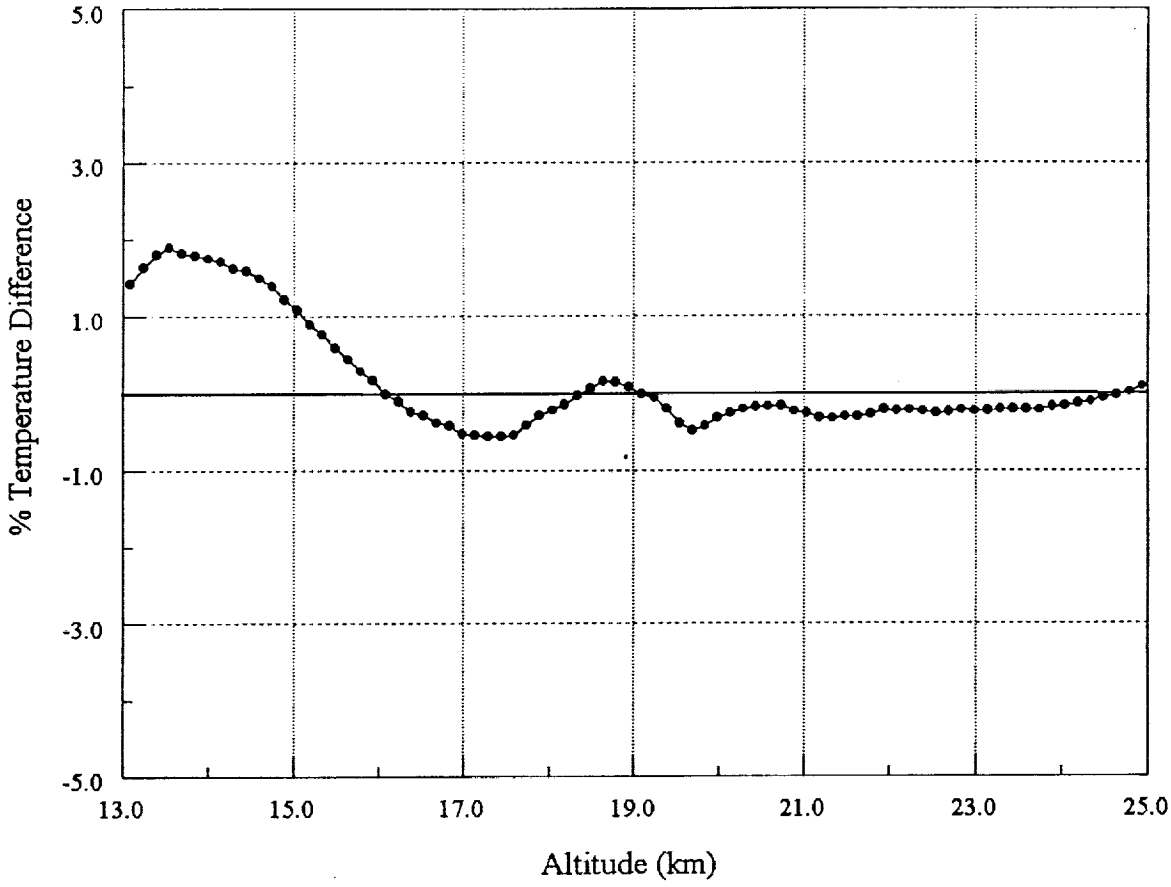

Figure 8 Differences between elastic and inelastically derived temperatures for 991212 calculated between 13 and 25 km altitude and averaged over the entire flight. From 20 through 25 km the differences averaged <0.3%.

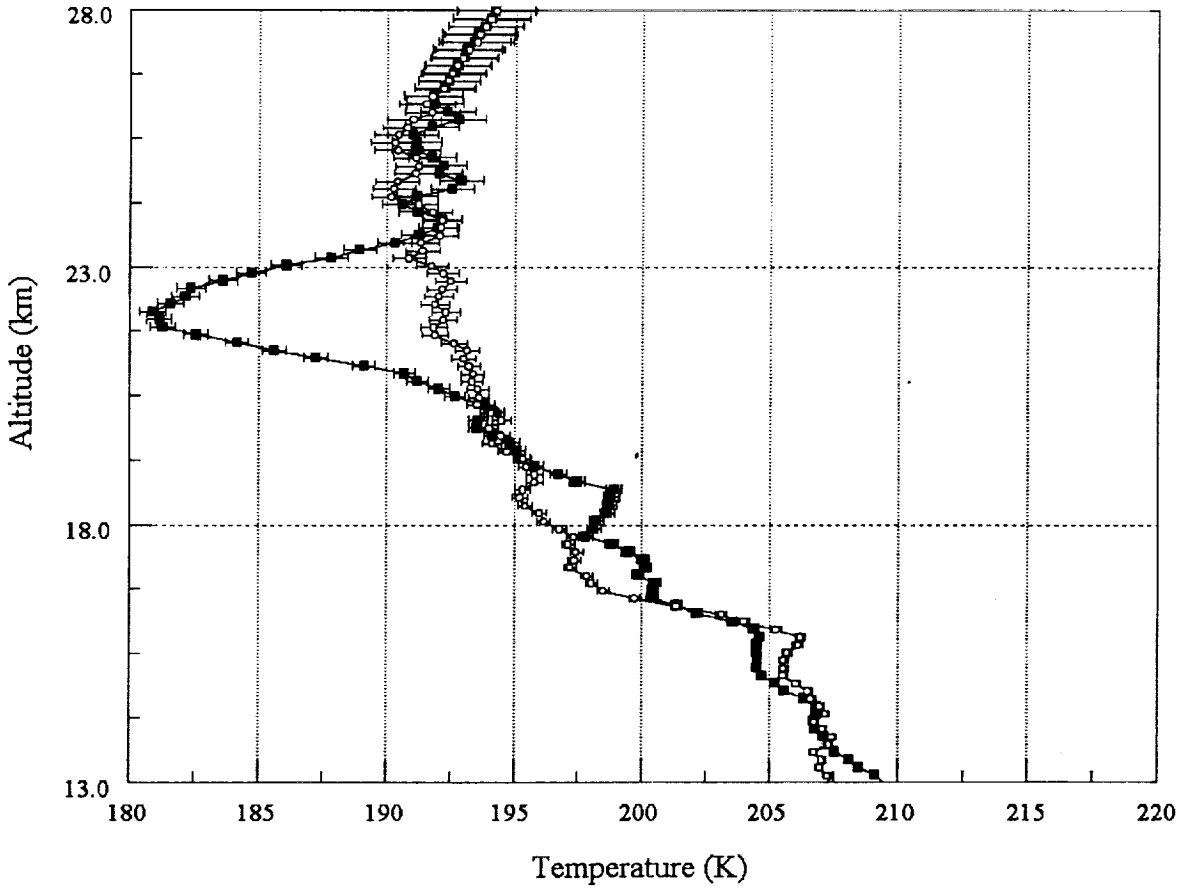

Figure 9 Elastic (solid squares) and inelastically (open squares) derived temperatures within an optically thin PSC on 991207. 1-sigma uncertainties are shown.

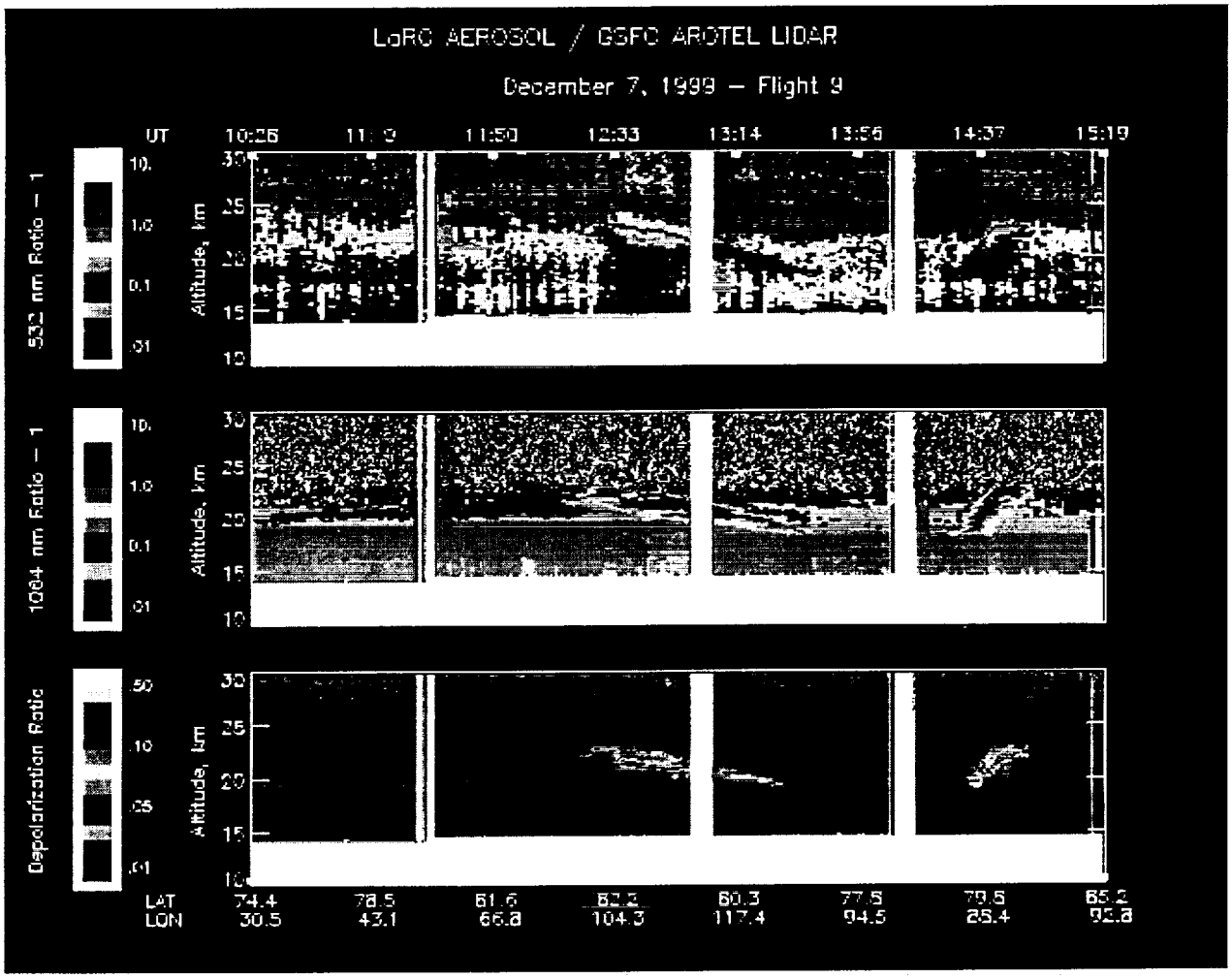

Figure 10 PSC profiles as a function of time (GMT) and altitude for flight date 991207.

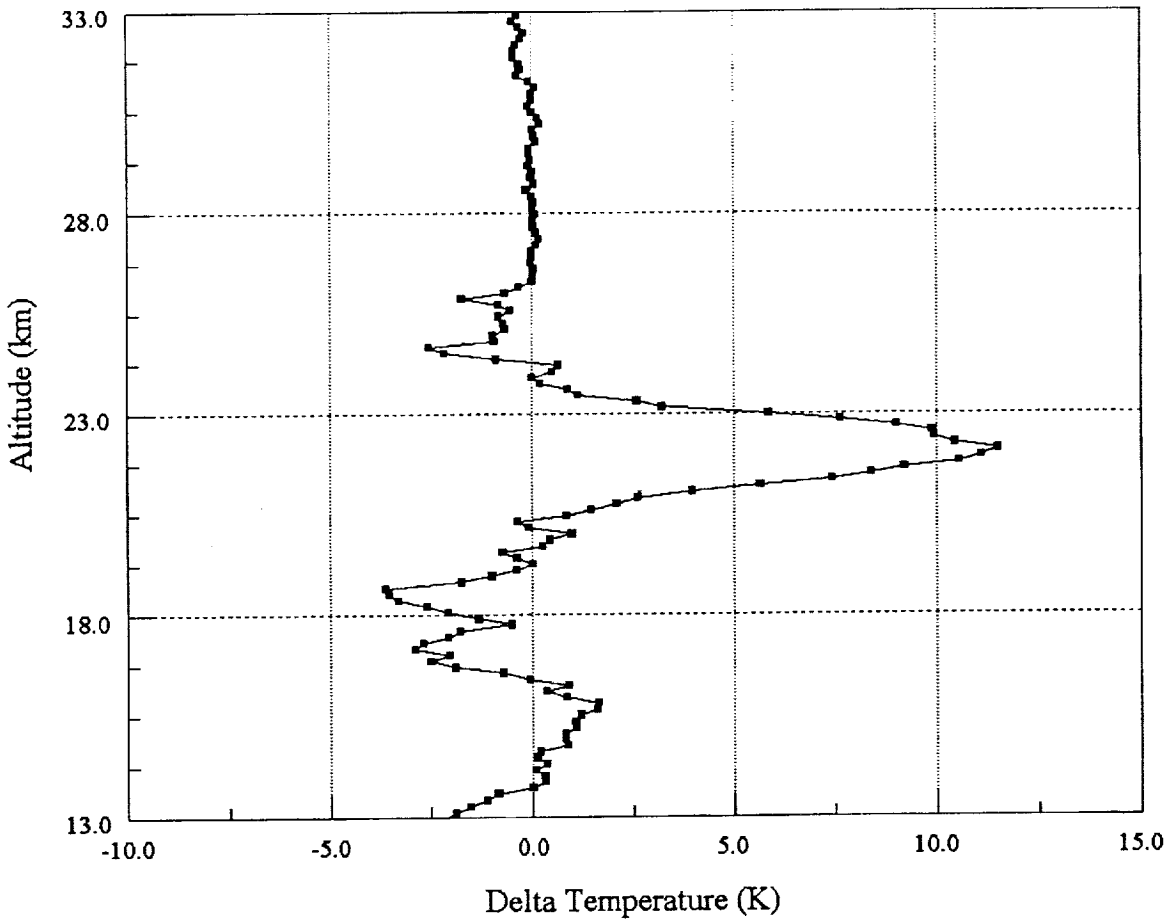

Figure 11 Differences between elastic and inelastically derived temperatures acquired simultaneously within an optically thin PSC on 991207.

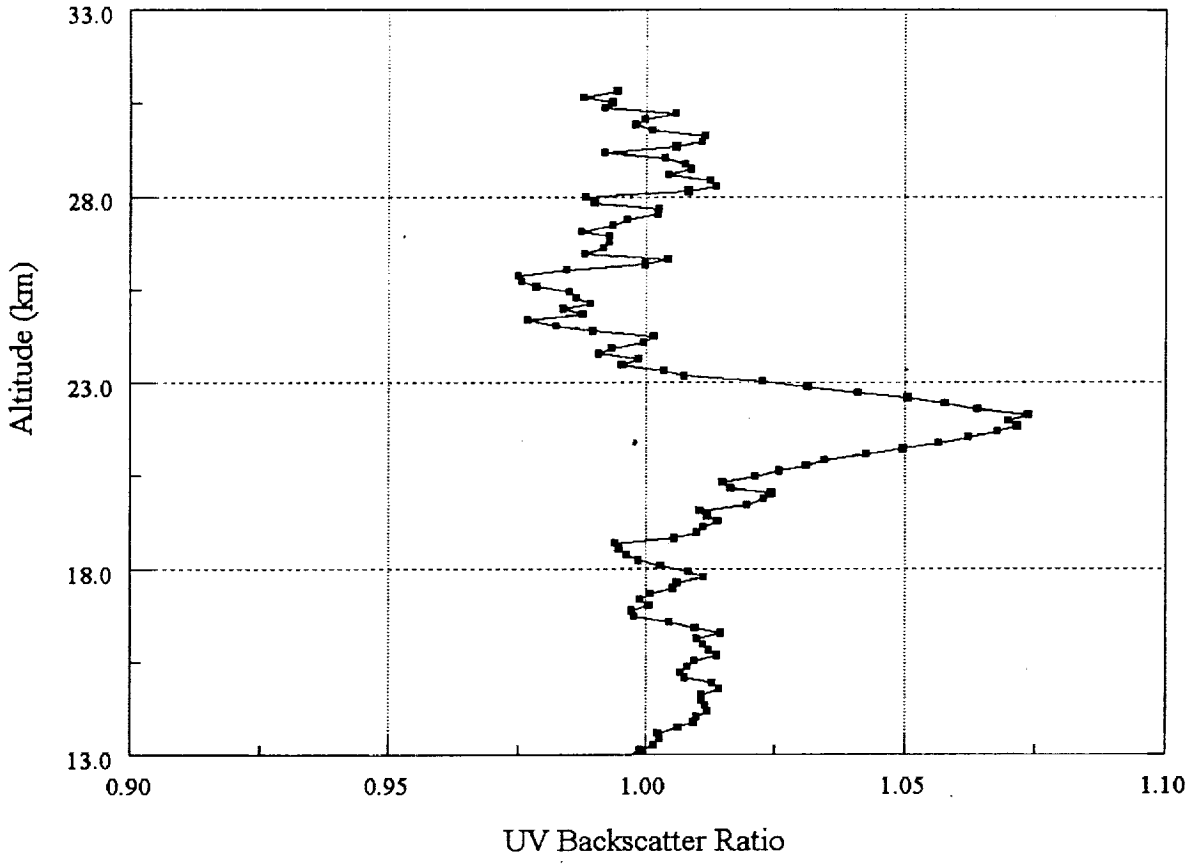

Figure 12 Backscatter ratio at 355 nm within a PSC on 991207. The peak value of ~1.07 identifies this as an optically thin cloud.

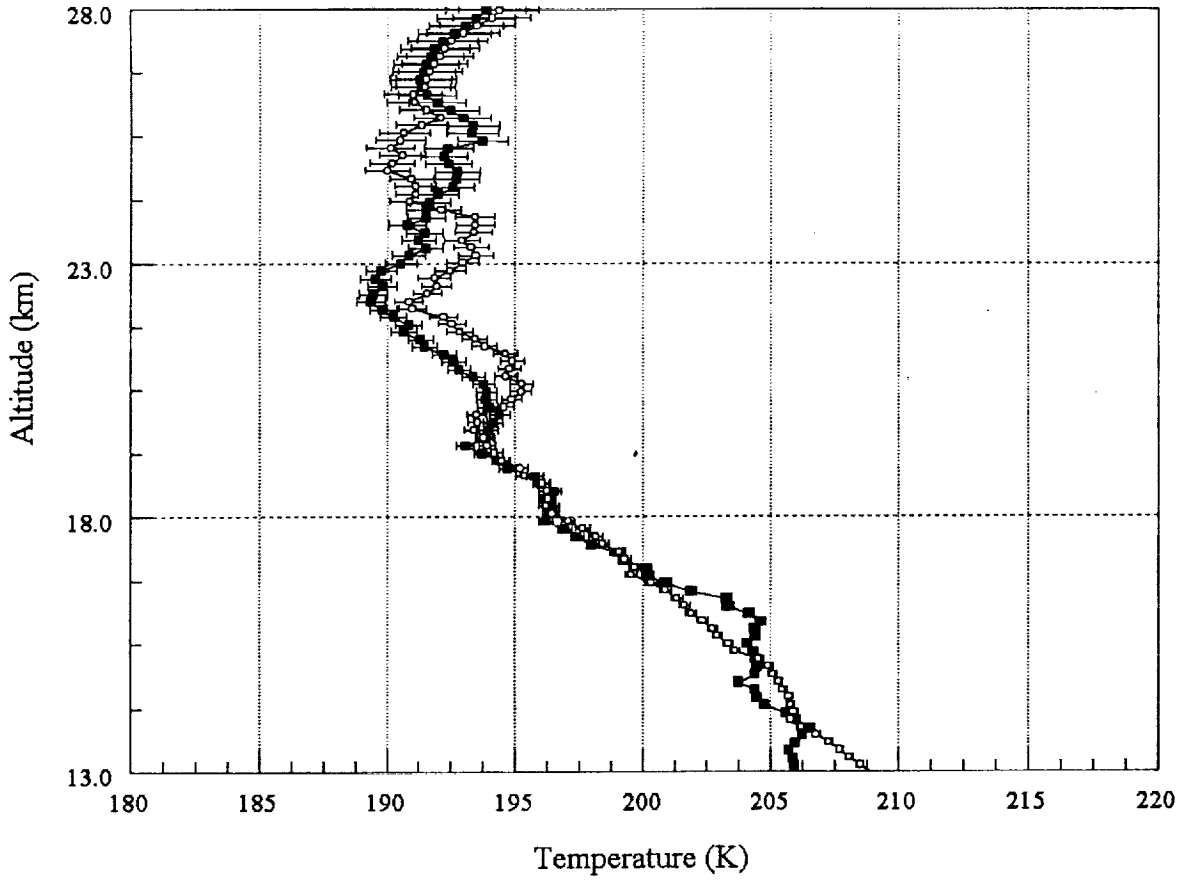

Figure 13 Elastic (open squares) and inelastically (solid squares) derived temperatures just outside the PSC detected on 991207. Error bars are 1-sigma.

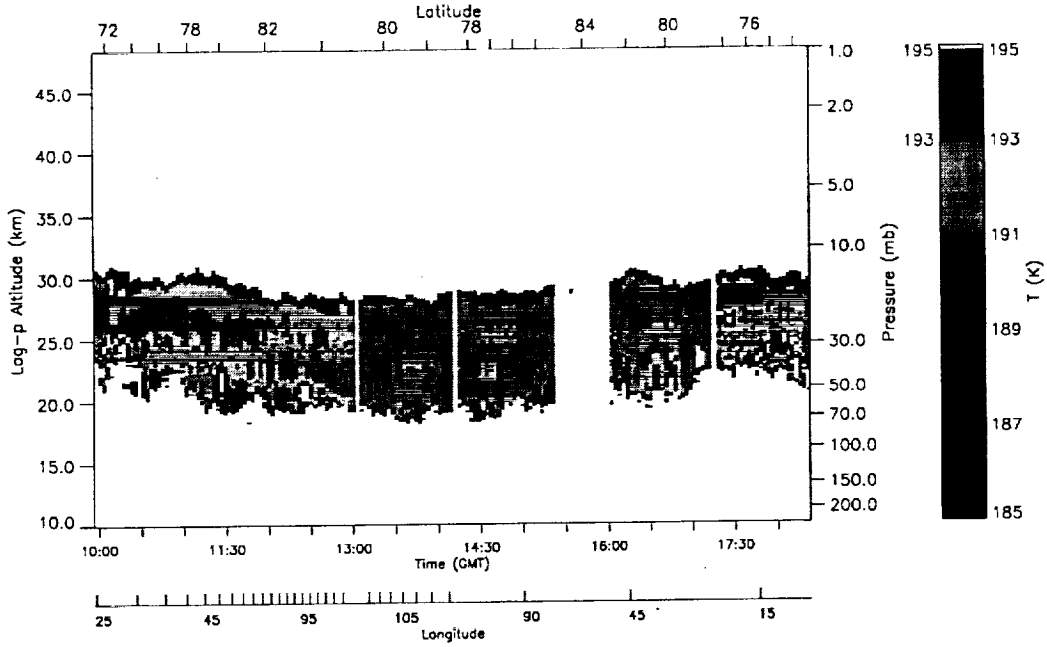

Figure 14 High resolution elastic temperatures between 185 K and 195 K for flight date 991207. Although PSCs were observed temperatures were not as cold on this date as on 991212.

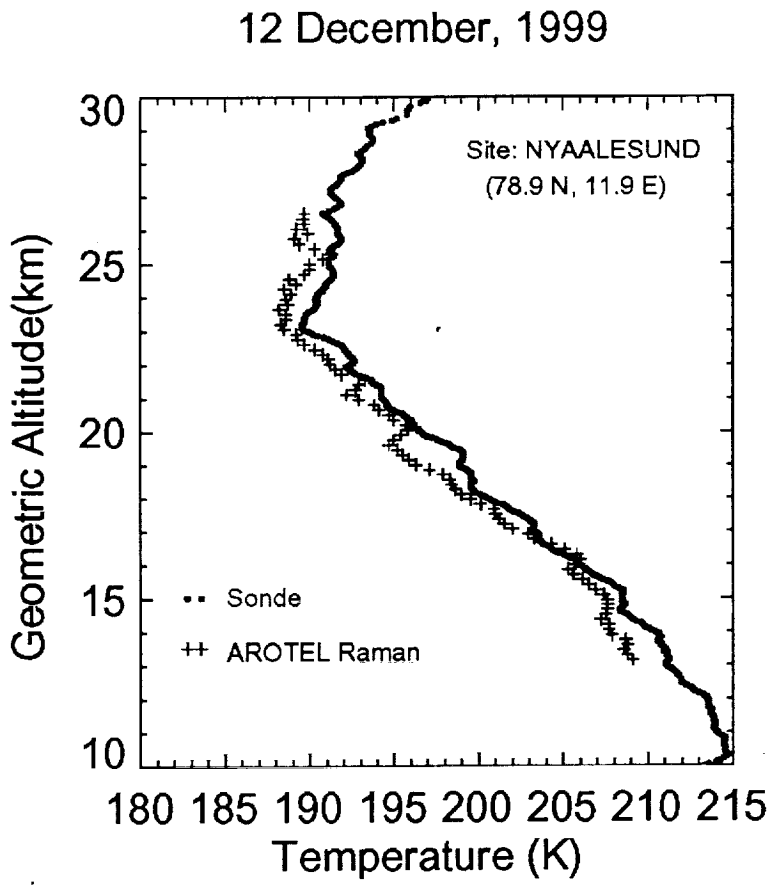

Figure 15 Balloon sonde and AROTEL temperatures (inelastically derived data) for 991212. The AROTEL profile was acquired on 17.36 GMT, the sonde was launched from Ny Ålesund at 16.03 GMT. The minimum sonde temperature was ~189 K at 23 km, AROTEL measured ~188 K for this altitude.

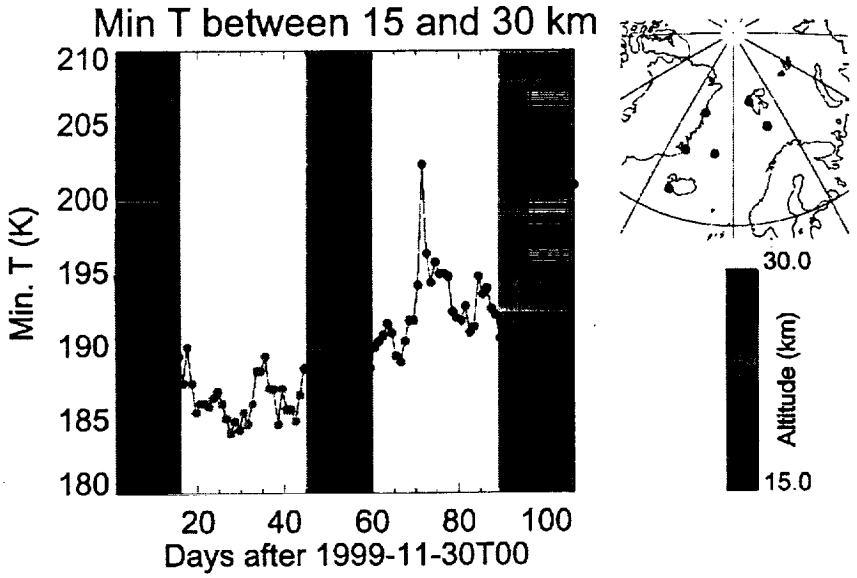

Figure 16 Minimum temperatures versus date and altitude for sondes launched from Ny Ålesund (78.9N, 11.9E), Danmarkshaven, Greenland (76.8N, 18.8W), Scoresbysund, Greenland (70.5N, 22.0W), Jan Mayen, Norway (70.9N, 8.7W), Bjornoya Island, Norway (74.5N, 19.0E),and Keflavik, Iceland (64.0N, 22.6W) from November 30, 1999 through March 15, 2000.

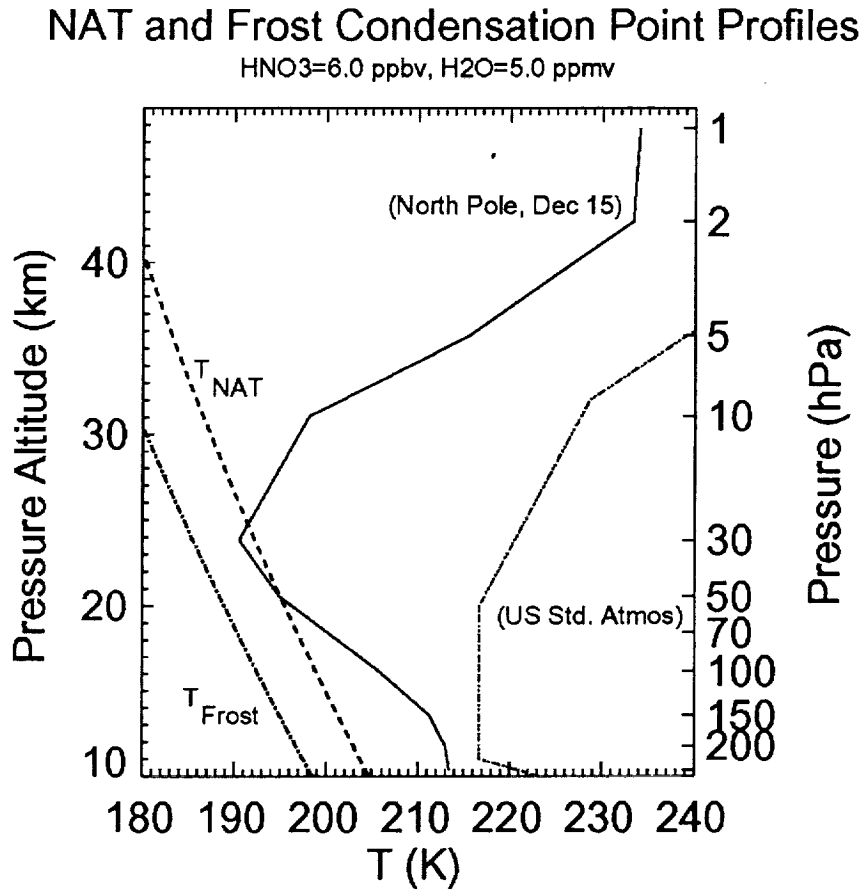

Figure 17 T_{nat} (dashed line) and T_{sat} (dot-dash line) as a function of altitude for 6 ppbv of nitric acid and 5 ppmv water. The solid line is a model profile of temperature at the North Pole on 12/15, the dot-dash line is the US Standard Atmosphere temperature.

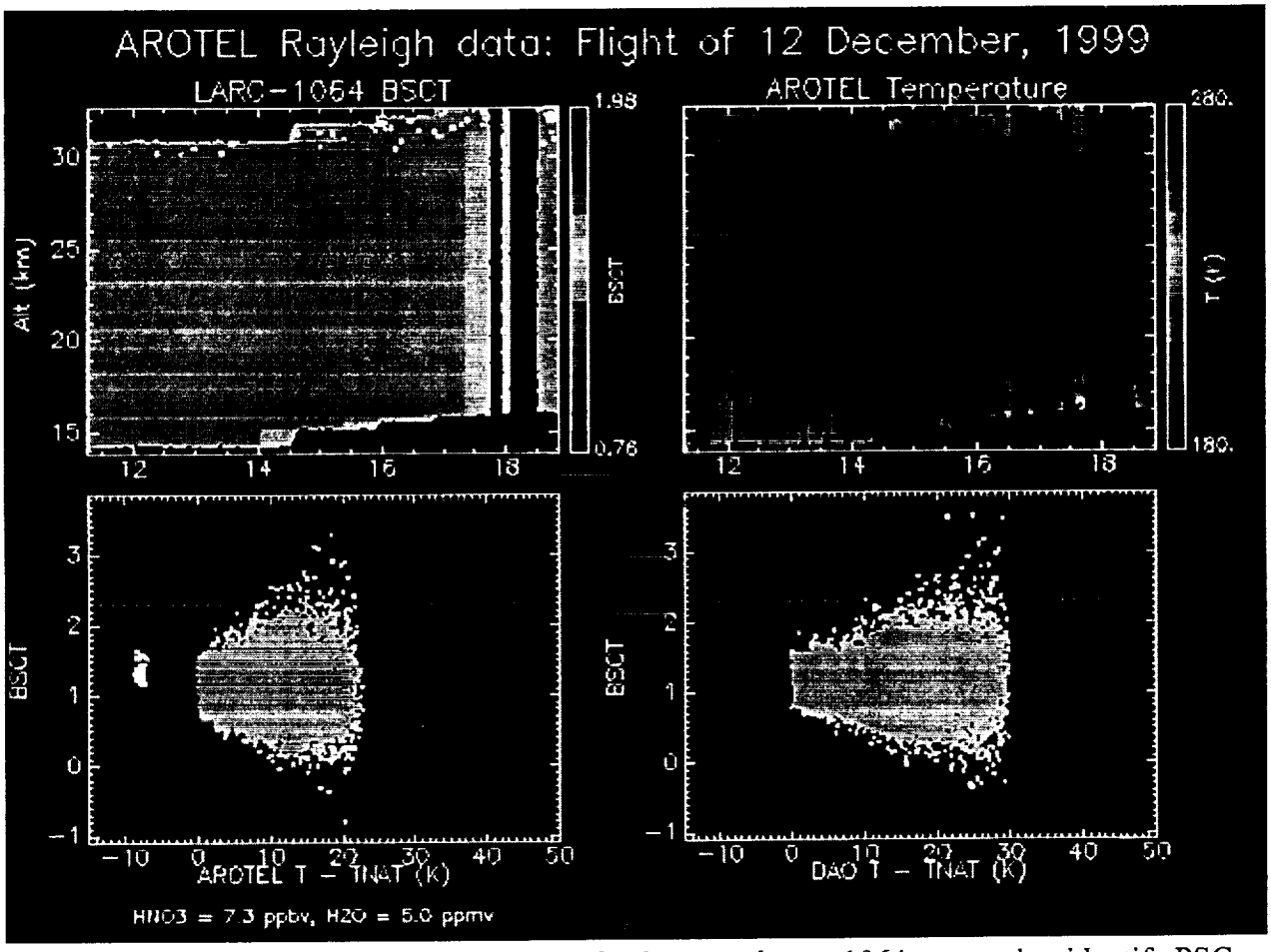

Figure 18 The upper left plot is of LaRC backscatter data at 1064 nm used to identify PSCs. The upper right plot is of AROTEL temperatures for the same altitude range as the LaRC data. The lower left plot displays the backscatter ratio data measured by LaRC as a function of $T_{AROTEL} - T_{NAT}$. The red area highlights conditions where type 1 PSCs could exist for AROTEL temperatures and measured values of nitric acid and water. The yellow region highlights where type 2 PSCs could exist. The dotted line delineates the regions where PSCs were observed from where they were not. The lower right plot is identical to that on the left except for the use of DAO, rather than AROTEL, temperatures for the PSC existence calculation.

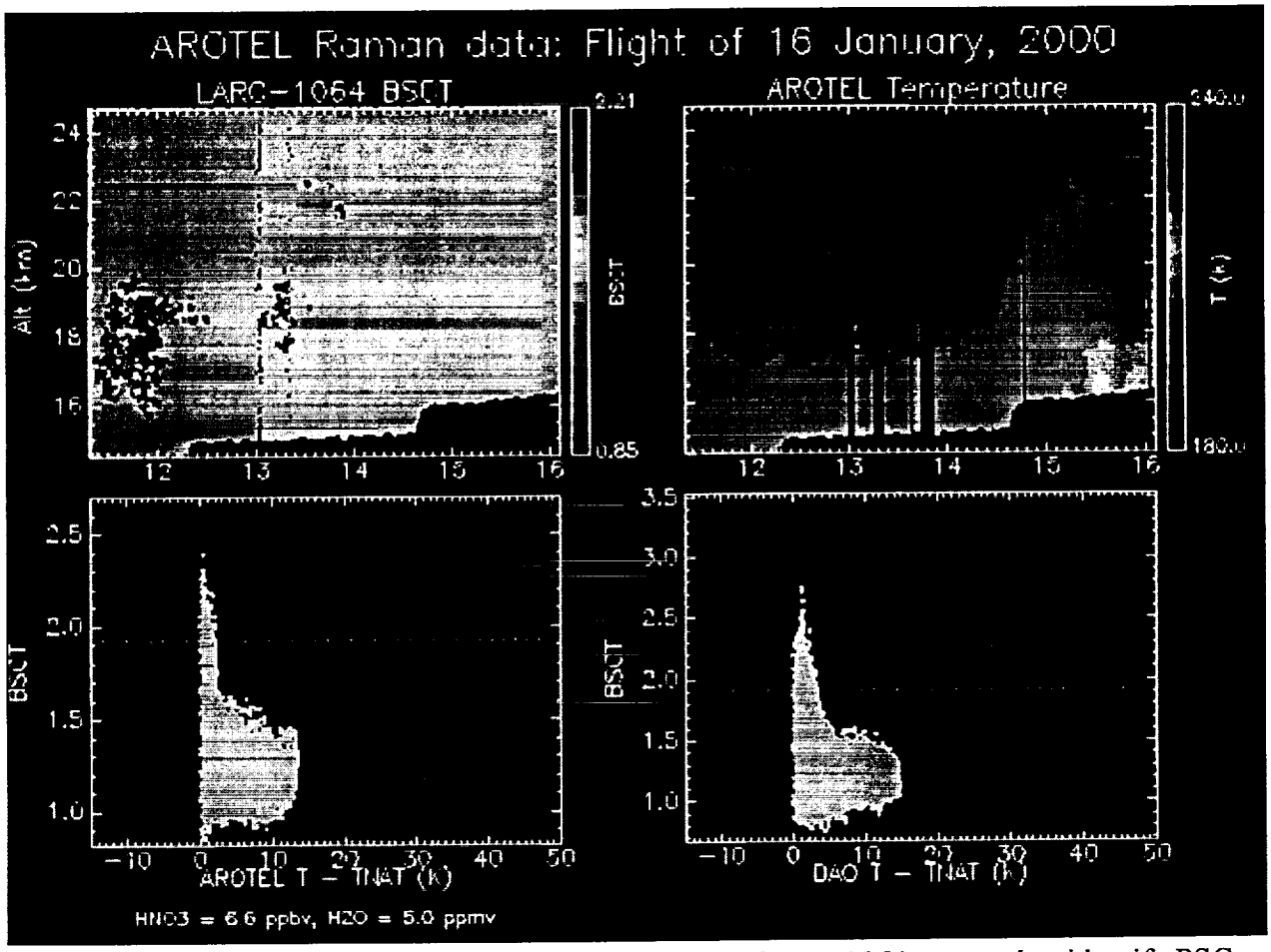

Figure 19 The upper left plot is of LaRC backscatter data at 1064 nm used to identify PSCs. The upper right plot is of AROTEL temperatures for the same altitude range as the LaRC data. The lower left plot displays the backscatter ratio data measured by LaRC as a function of $T_{AROTEL} - T_{NAT}$. The red area highlights conditions where type 1 PSCs could exist for AROTEL temperatures and measured values of nitric acid and water. The yellow region highlights where type 2 PSCs could exist. The dotted line delineates the regions where PSCs were observed from where they were not. The lower right plot is identical to that on the left except for the use of DAO, rather than AROTEL, temperatures for the PSC existence calculation.

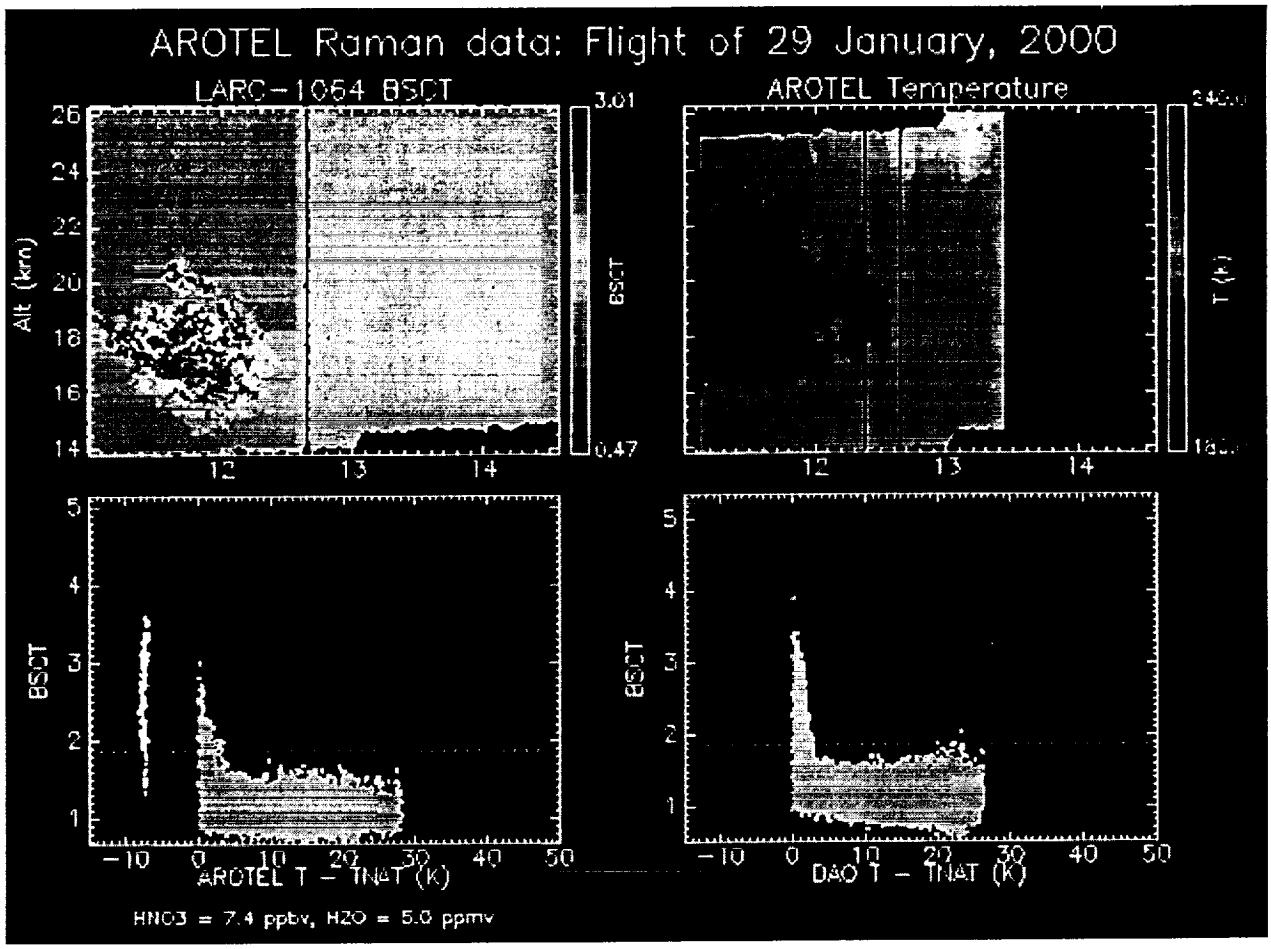

Figure 20 The upper left plot is of LaRC backscatter data at 1064 nm used to identify PSCs. The upper right plot is of AROTEL temperatures for the same altitude range as the LaRC data. The lower left plot displays the backscatter ratio data measured by LaRC as a function of $T_{AROTEL} - T_{NAT}$. The red area highlights conditions where type 1 PSCs could exist for AROTEL temperatures and measured values of nitric acid and water. The yellow region highlights where type 2 PSCs could exist. The dotted line delineates the regions where PSCs were observed from where they were not. The lower right plot is identical to that on the left except for the use of DAO, rather than AROTEL, temperatures for the PSC existence calculation.